Acta Crystallographica Section D
Biological Crystallography
ISSN 0907-4449

Structural basis for compound C inhibition of the human AMP-activated protein kinase α2 subunit kinase domain

**Noriko Handa,[a] Tetsuo Takagi,[a] Shinya Saijo,[a]‡ Seiichiro Kishishita,[a] Daisuke Takaya,[a] Mitsutoshi Toyama,[a] Takaho Terada,[a] Mikako Shirouzu,[a] Atsushi Suzuki,[b] Suni Lee,[b] Toshimasa Yamauchi,[c] Miki Okada-Iwabu,[c] Masato Iwabu,[c] Takashi Kadowaki,[c] Yasuhiko Minokoshi[b] and Shigeyuki Yokoyama[a,d,e]*

[a]RIKEN Systems and Structural Biology Center, 1-7-22 Suehiro-cho, Tsurumi, Yokohama 230-0045, Japan, [b]Division of Endocrinology and Metabolism, Department of Developmental Physiology, National Institute for Physiological Sciences, 38 Nishigonaka, Myodaiji, Okazaki, Aichi 444-8585, Japan, [c]Department of Diabetes and Metabolic Diseases, Graduate School of Medicine, The University of Tokyo, Bunkyo-ku, Tokyo 113-0033, Japan, [d]Department of Biophysics and Biochemistry, Graduate School of Science, The University of Tokyo, Bunkyo-ku, Tokyo 113-0033, Japan, and [e]Laboratory of Structural Biology, Graduate School of Science, The University of Tokyo, Bunkyo-ku, Tokyo 113-0033, Japan

‡ Present address: Department of Biological Science and Technology, Tokyo University of Science, 2641 Yamazaki, Noda-shi, Chiba 278-8510, Japan.

Correspondence e-mail: yokoyama@biochem.s.u-tokyo.ac.jp

Received 2 December 2010
Accepted 17 March 2011

PDB References: T172D mutant AMPK α2 kinase domain, apo form, 2yza; complex with compound C, 3aqv.

AMP-activated protein kinase (AMPK) is a serine/threonine kinase that functions as a sensor to maintain energy balance at both the cellular and the whole-body levels and is therefore a potential target for drug design against metabolic syndrome, obesity and type 2 diabetes. Here, the crystal structure of the phosphorylated-state mimic T172D mutant kinase domain from the human AMPK α2 subunit is reported in the apo form and in complex with a selective inhibitor, compound C. The AMPK α2 kinase domain exhibits a typical bilobal kinase fold and exists as a monomer in the crystal. Like the wild-type apo form, the T172D mutant apo form adopts the autoinhibited structure of the 'DFG-out' conformation, with the Phe residue of the DFG motif anchored within the putative ATP-binding pocket. Compound C binding dramatically alters the conformation of the activation loop, which adopts an intermediate conformation between DFG-out and DFG-in. This induced fit forms a compound-C binding pocket composed of the N-lobe, the C-lobe and the hinge of the kinase domain. The pocket partially overlaps with the putative ATP-binding pocket. These three-dimensional structures will be useful to guide drug discovery.

1. Introduction

Mammalian AMP-activated protein kinase (AMPK) acts as a 'fuel gauge' that monitors cellular energy status. It is activated under circumstances with an increased cellular AMP:ATP ratio, such as metabolic stresses that inhibit ATP production (hypoxia, glucose deprivation, metabolic inhibitors *etc.*) and those that stimulate ATP consumption (exercise, cell growth and division *etc.*) (Hardie, 2007). In addition, it is regulated by hormones (Minokoshi *et al.*, 2002, 2004; Yamauchi *et al.*, 2002; Suzuki *et al.*, 2007), growth factors (Suzuki *et al.*, 2004, 2005) and antidiabetic drugs (Zhou *et al.*, 2001). Inhibition of hypothalamic AMPK by leptin and insulin reduces food intake (Minokoshi *et al.*, 2004). The activation of AMPK leads to the phosphorylation of downstream targets and thus switches on ATP-producing pathways and switches off ATP-consuming pathways. AMPK is a heterotrimer consisting of one catalytic subunit (α) and two regulatory subunits (β and γ). Two α-subunit isoforms, α1 and α2, exist in mammals, with 90 and 61% amino-acid sequence identity within the catalytic domain and the remaining C-terminal half region, respectively (Stapleton *et al.*, 1996). The α2 isoform is abundant in cardiac and skeletal muscle (70–80% of the total AMPK activity; Cheung *et al.*, 2000). Phosphorylation of the activation-loop threonine (Thr172 of α2) or allosteric modulation by AMP binding is essential for AMPK activation (Hardie *et al.*, 2006). It has been postulated that LKB1, Ca^{2+}/calmodulin-dependent

Table 1
Data-collection, phasing and refinement statistics.

Values in parentheses are for the highest resolution shell.

Data set	Apo	Compound C complex
Data collection and processing		
Wavelength (Å)	1.000	1.000
Resolution range (Å)	25–3.0	50–2.08
Unique reflections	4913	20469
Measured reflections	14927	246701
Multiplicity	3.0	12.1
Completeness (%)	94.3 (51.6)	99.9 (100.0)
$R_{\rm merge}$† (%)	10.6 (25.1)	7.2 (40.9)
$\langle I/\sigma(I)\rangle$	11.5 (3.2)	34.2 (8.1)
Model refinement		
Resolution range (Å)	25–3.02	20–2.08
No. of reflections	4422	19340
No. of protein atoms	2063	2158
No. of water molecules	10	112
No. of compound C atoms	0	30
$R_{\rm work}/R_{\rm free}$‡ (%)	22.7/30.8	22.1/28.1
Stereochemistry		
R.m.s.d. for bond lengths (Å)	0.006	0.023
R.m.s.d. for bond angles (°)	0.873	2.071
Residues in the Ramachandran plot		
Most favoured region (%)	92.9	89.2
Additional allowed regions (%)	7.1	10.3
Generously allowed regions (%)	0	0.4
Disallowed regions (%)	0	0

† $R_{\rm merge} = \sum_{hkl}\sum_i |I_i(hkl) - \langle I(hkl)\rangle|/\sum_{hkl}\sum_i I_i(hkl)$, where hkl indicates unique reflection indices and i indicates symmetry-equivalent indices. ‡ $R_{\rm work} = \sum_{hkl} ||F_{\rm obs}| - |F_{\rm calc}||/\sum_{hkl}|F_{\rm obs}|$ for all reflections; $R_{\rm free}$ was calculated using randomly selected reflections (5%).

protein kinase kinase, ATM and TAK1 are AMPK kinases (Alessi *et al.*, 2006; Hawley *et al.*, 2005; Hurley *et al.*, 2005; Suzuki *et al.*, 2004; Momcilovic *et al.*, 2006; Woods *et al.*, 2005).

Crystal structures of the kinase domain of the AMPK homologue from *Saccharomyces cerevisiae*, Snf1, have been reported by two groups (Nayak *et al.*, 2006; Rudolph *et al.*, 2005). The kinase domain adopts a typical kinase fold and forms a dimer in the crystals. The homodimeric structure is considered to represent an inactive form of the kinase (Nayak *et al.*, 2006). Structures of the *Schizosaccharomyces pombe* AMPK α subunit KD-AID, which contains the kinase domain and the autoinhibitory domain, have been reported (Chen *et al.*, 2009). The autoinhibitory domain interacts with the hinge of the kinase domain from the 'back side' and limits the movement of the αC helix, thus inhibiting the kinase activity (Chen *et al.*, 2009). Recently, the crystal structure of the wild-type human AMPK α2 kinase domain has been reported (Littler *et al.*, 2010). This kinase domain also adopts a typical kinase fold. In the structure, the aromatic ring of Phe158 in the DFG motif of the activation loop is anchored within the ATP-binding pocket and the kinase domain adopts the auto-inhibited structure of the 'DFG-out' conformation (Littler *et al.*, 2010).

Three structural studies of the AMPK heterotrimer core have been reported: the AMPK homologue from *S. pombe* (Townley & Shapiro, 2007), Snf1 from *S. cerevisiae* (Amodeo *et al.*, 2007) and the mammalian AMPK (Xiao *et al.*, 2007). All three structures contained full-length γ subunits and the C-terminal regions of the α and β subunits, but lacked the kinase domain of the α subunit. These structures revealed how the α, β and γ subunits interact with each other and how AMP molecules bind to the nucleotide-binding pockets in the γ subunit.

Compound C ({6-[4-(2-piperidin-1-yl-ethoxy)-phenyl]}-3-pyridin-4-yl-pyrazolo[1,5-*a*]pyrimidine) is a selective inhibitor of AMPK (Zhou *et al.*, 2001). Intracerebroventricular or intraperitoneal injection of compound C in mice reduces food intake (Kim *et al.*, 2004). Furthermore, in mouse models of central nervous system ischaemia, intraperitoneally injected compound C reduces stroke damage (McCullough *et al.*, 2005). Mice deficient in the AMPK α2 subunit demonstrate reduced infarct volume, whereas mice deficient in the AMPK α1 subunit show no effect (Li *et al.*, 2007). Thus, AMPK inhibitors may be effective in the treatment of obesity and cerebral infarction. On the other hand, AMPK activators might be useful for managing metabolic diseases, including type 2 diabetes and cardiovascular disease, because of the stimulation of energy consumption by AMPK (Fogarty & Hardie, 2010). In addition, recent reports have suggested that AMPK activators may also potentially function as anticancer drugs (Fogarty & Hardie, 2010).

Here, we report crystal structures of the T172D mutant human AMPK α2 kinase domain, which mimics the phosphorylated state, in the apo form and in complex with compound C. The structure of the apo AMPK α2 kinase domain exhibits the 'DFG-out' conformation and is essentially identical to that of the wild type. The structure obtained from cocrystallization with compound C adopts an intermediate conformation between 'DFG-out' and 'DFG-in', revealing a novel inhibitor-binding mode of the unique activation-loop conformation.

2. Materials and methods

2.1. Protein expression and purification

The T172D mutant of the human AMPK α2 gene was produced by QuikChange site-directed mutagenesis (Stratagene, La Jolla, California, USA) and was verified by DNA sequencing. The kinase domain (residues 6–279) of the human AMPK α2 mutant with an N-terminal histidine-affinity tag and a tobacco etch virus (TEV) protease cleavage site was synthesized by the *Escherichia coli* cell-free system using the dialysis method (Kigawa *et al.*, 2004; Kigawa, Yabuki & Yokoyama, 1999; Kigawa, Yabuki, Yoshida *et al.*, 1999; Wada *et al.*, 2003). The protein was purified by chromatography on a HiTrap Chelating column (GE Healthcare Bio-Sciences) and was subjected to TEV protease digestion. The protein sample was subsequently purified using a Superdex 75 (GE Healthcare Bio-Sciences) column.

2.2. Crystallization

Crystals of the apo AMPK α2 kinase-domain mutant (T172D) were grown at 293 K by the hanging-drop vapour-diffusion method. The protein concentration was 2.8 mg ml^{-1}

in 20 m*M* Tris–HCl buffer pH 8.5 containing 0.3 *M* NaCl, 10% glycerol, 2 m*M* DTT, 5 m*M* $MgCl_2$ and 5 m*M* AMPPNP. The reservoir solution consisted of 0.1 *M* Tris–HCl pH 8.9, 15% 2-propanol, 0.1 *M* ammonium sulfate and 16% PEG 4000. The crystals belonged to space group $P2_1$, with unit-cell parameters a = 39.19, b = 67.34, c = 50.65 Å, β = 91.26°. There is one monomer in the asymmetric unit. X-ray diffraction data were collected on BL26B2 at SPring-8 (Harima, Japan).

Crystals of the AMPK α2 kinase-domain mutant (T172D) complexed with compound C were grown at 293 K using the sitting-drop vapour-diffusion method. The protein concentration was 2.8 mg ml^{-1} in 20 m*M* Tris–HCl buffer pH 8.5 containing 0.3 *M* NaCl, 10% glycerol, 2 m*M* DTT, 5 m*M* $MgCl_2$ and 0.5 m*M* compound C. The reservoir solution consisted of 0.1 *M* Bis-Tris pH 6.5, 1.5 *M* ammonium sulfate and 0.1 *M* NaCl. The crystals belonged to space group $P4_32_12$, with unit-cell parameters $a = b$ = 70.48, c = 130.51 Å. There is one monomer in the asymmetric unit. X-ray diffraction data were collected on NW12A at PF-AR (Tsukuba, Japan).

All data were processed using the *HKL*-2000 and *SCALEPACK* programs (Otwinowski & Minor, 1997). The data-processing statistics are summarized in Table 1.

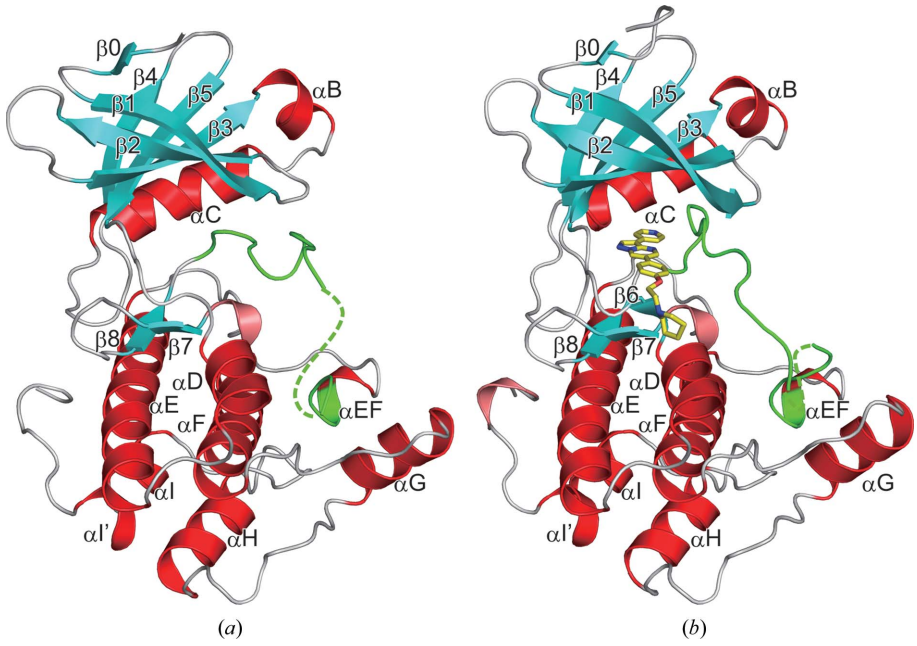

Figure 1
Ribbon diagrams of the kinase domain of the AMPK α2 subunit mutant (T172D) in the apo form (*a*) and in the compound C complex (*b*). α-Helices are shown in red, β-strands in cyan, 3_{10}-helices in salmon and random coils in grey. The activated loop is shown in green. Disordered regions are represented by dotted lines. The bound compound C molecule is represented by a stick model, with C, O and N atoms shown in yellow, red and blue, respectively.

2.3. Structure determination and refinement

The structure of the apo form was determined by molecular replacement with *MOLREP* (Vagin & Teplyakov, 2010) using the coordinates of the wild-type human AMPK α2 kinase domain (PDB entry 2h6d; Littler *et al.*, 2010). The model was built using *TURBO-FRODO* (http://www.afmb.univ-mrs.fr/-TURBO-) and was refined using *REFMAC* v.5.2 (Winn *et al.*, 2001). In the electron-density map, the N-terminal artificial linker and the following four residues, residues 167–177 in the activation loop and the C-terminal residue were disordered. The structure is essentially identical to that of the wild type.

The compound C complex structure was determined by molecular replacement with *MOLREP* using the coordinates of the T172D mutant apo-form structure. The model was built using *TURBO-FRODO* and was refined using *CNS* v.1.1 and *REFMAC* v.5.2 (Brünger *et al.*, 1998; Winn *et al.*, 2001). In the electron-density map, the N-terminal artificial linker and the following residue and residues 171–174 in the activation loop were disordered. The refinement statistics are summarized in Table 1. The ribbon, tube, stick and solvent-accessible surface models in the figures were drawn using *PyMOL* (http://pymol.sourceforge.net/).

2.4. Docking

The binding mode of STO 609 to AMPK was predicted by a molecular-docking algorithm using the compound-C-complexed structure. Docking calculations were performed with the program *Glide SP* (Friesner *et al.*, 2004). In the docking process, we introduced a constraint for a hydrogen-bonding interaction of Val96 in the hinge region because a similar hydrogen-bonding interaction with ATP is conserved in the kinase family. The highest scoring model of STO 609 docked in the compound-C binding pocket of AMPK is shown in Fig. 4(*d*).

3. Results

3.1. Overall structure of the kinase domain of the AMPK α2 subunit

The crystal structure of the kinase domain of the AMPK α2 subunit mutant (T172D), which mimics the phosphorylated state, has been determined in the apo form and in complex with compound C at 3.0 and 2.08 Å resolution, respectively. The phosphorylation of Thr172 in the activation loop is essential for kinase activation (Cheung *et al.*, 2000; Hardie *et al.*, 2006). The AMPK α1 isoform kinase domain alone exhibits the same activity as the entire AMPK heterotrimer (Scott *et al.*, 2002). The activity of the T172D mutant kinase domain with and without AMPK kinase is about 40-fold higher than that of the wild-type kinase domain treated with protein phosphatase 2A (Scott *et al.*, 2002).

The kinase-domain structures display the typical bilobal protein-kinase fold (Fig. 1). The N-terminal lobe consists of a twisted six-stranded antiparallel β-sheet (β0–β5) and two α-helices (αB and αC; Figs. 1 and 2). The C-terminal lobe is composed of eight α-helices (αD, αE, αEF, αF, αG, αH, αI and αI′). In addition, β6, found in Snf1, is also present in the compound-C-complexed form, whereas it is not present in the apo form. The electron density around the phosphothreonine mimic Asp172 was not visible in either the apo form or the compound-C-complexed form; however, the activation loop of the apo form is more flexible than that of the compound-C-complexed form, as judged by the electron density and the *B* factors.

The apo-form structure of the T172D mutant is essentially identical to that published recently for the wild type (Littler *et al.*, 2010). The DFG motif is flipped compared with the canonical DFG motifs of other kinases, such as the inactive form of Snf1 and the active form of CDK2 ($\varphi_{\mathrm{Asp157,\ AMPK\ \alpha2\ apo}} = -108^{\circ}$, $\varphi_{\mathrm{Asp195,\ Snf1}} = 71^{\circ}$, $\varphi_{\mathrm{Asp145,\ CDK2}} = 47^{\circ}$; Figs. 3*a* and 3*c*; Littler *et al.*, 2010). This inactive mode of Asp in the DFG motif is called the 'DFG-out' conformation, whereas the canonical DFG-motif conformation is referred to as the 'DFG-in' conformation (Pargellis *et al.*, 2002). The aromatic ring of Phe158 in the DFG motif is anchored within the putative ATP-binding pocket (Fig. 3*a*; Littler *et al.*, 2010). This explains why the ATP analogue AMPPNP could not be seen in the electron-density map when we added AMPPNP to the crystallization drops. As a result of this DFG-out conformation, the activation loop does not interact with either the αC helix or the catalytic loop (Figs. 1*a* and 3*a*). In the active conformation of the protein kinases, the DFG motif contacts the αC helix and the His-Arg-Asp (HRD) motif in the catalytic loop and forms ionic interactions with the conserved Lys–Glu pair (Fig. 3*c*; the His125–Phe146 and Lys33–Glu51 interactions in CDK2; Kannan & Neuwald, 2005; Ten Eyck *et al.*, 2008; Brown *et al.*, 1999).

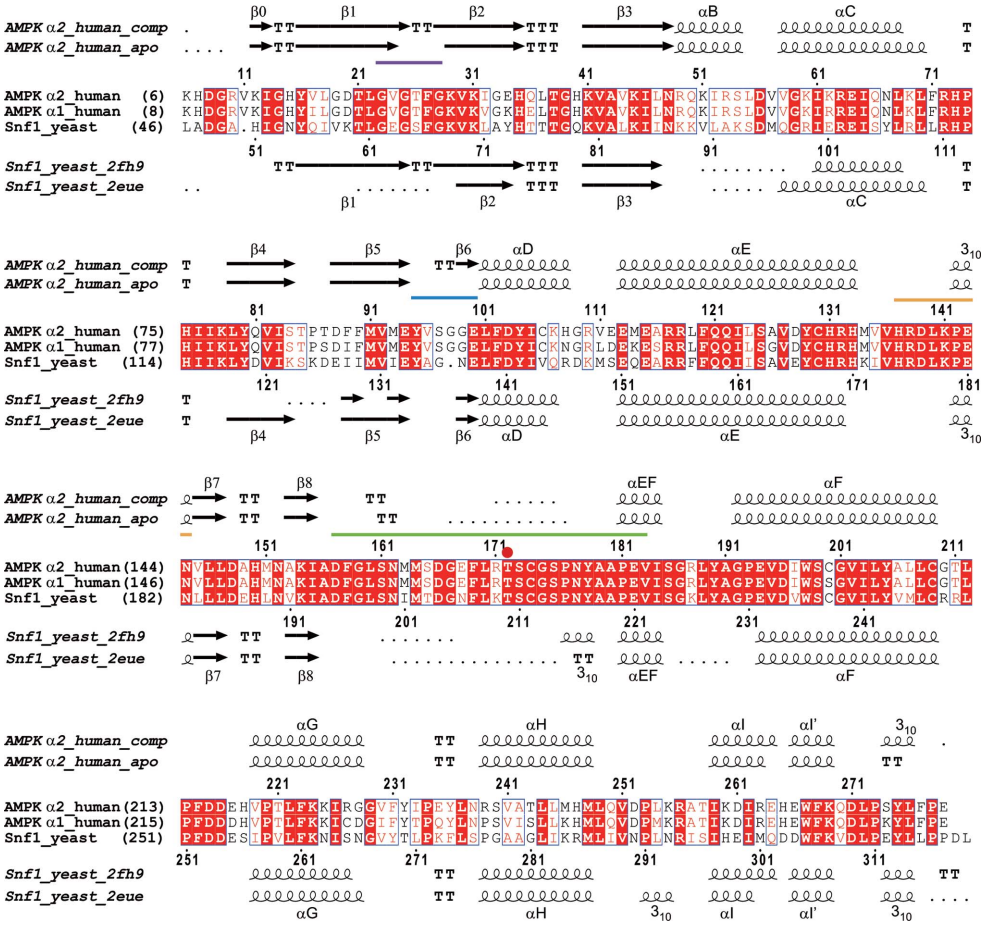

Figure 2
Sequence alignment of the AMPK/Snf1 kinase domains. Strictly conserved and similar residues are represented by white characters on a red background and by red characters, respectively. Secondary structures of the human AMPK α2 kinase complexed with compound C (*AMPK α2_human_comp*) and the human AMPK α2 kinase apo form (*AMPK α2_human_apo*) are indicated above the alignment. Secondary structures of the two Snf1 crystal structures are indicated below the alignment (PDB entry 2fh9, *Snf1_yeast_2fh9*, Nayak *et al.*, 20006; PDB entry 2eue, *Snf1_yeast_2eue*, Rudolph *et al.*, 2005). The glycine-rich loop (phosphate-binding loop), the hinge, the catalytic loop and the activation loop are indicated by purple, blue, orange and green bars, respectively. The Thr residue in the activation loop, which must be phosphorylated for kinase activation, is indicated by a red circle. The figure was generated using *ESPript* (Gouet *et al.*, 1999).

3.2. Compound C inhibition of the AMPK α2 kinase domain

The bound compound C molecule, with the exception of the piperidine ring, was unambiguously identified in the electron-density map (Fig. 4*a*). The piperidine ring resides outside the binding pocket and is relatively flexible, but the remainder of the compound C molecule is fixed within the pocket (Figs. 4*b* and 4*c*). Compound C binds to a unique pocket formed by the N-lobe, the C-lobe and the hinge of the kinase domain (Fig. 4*b*). The pocket overlaps partially with the ATP-binding pocket seen in typical kinase domains such as CDK2 (Figs. 3*b* and 3*c*). Compound C forms a hydrogen bond and several hydrophobic and van der Waals interactions with the protein (Fig. 4*c*). The residues involved in this interface are Ala43 and Lys45 from the N-lobe, Tyr95 and Val96 from the hinge region and Gly99, Asp103, Tyr104, Lys107, Leu146, Ala156 and Met164 from the C-lobe (Fig. 4*c*). The pyrrazolo[1,5-*a*]-pyrimidine ring of compound C is fixed in the corresponding region of the ATP-binding pocket of

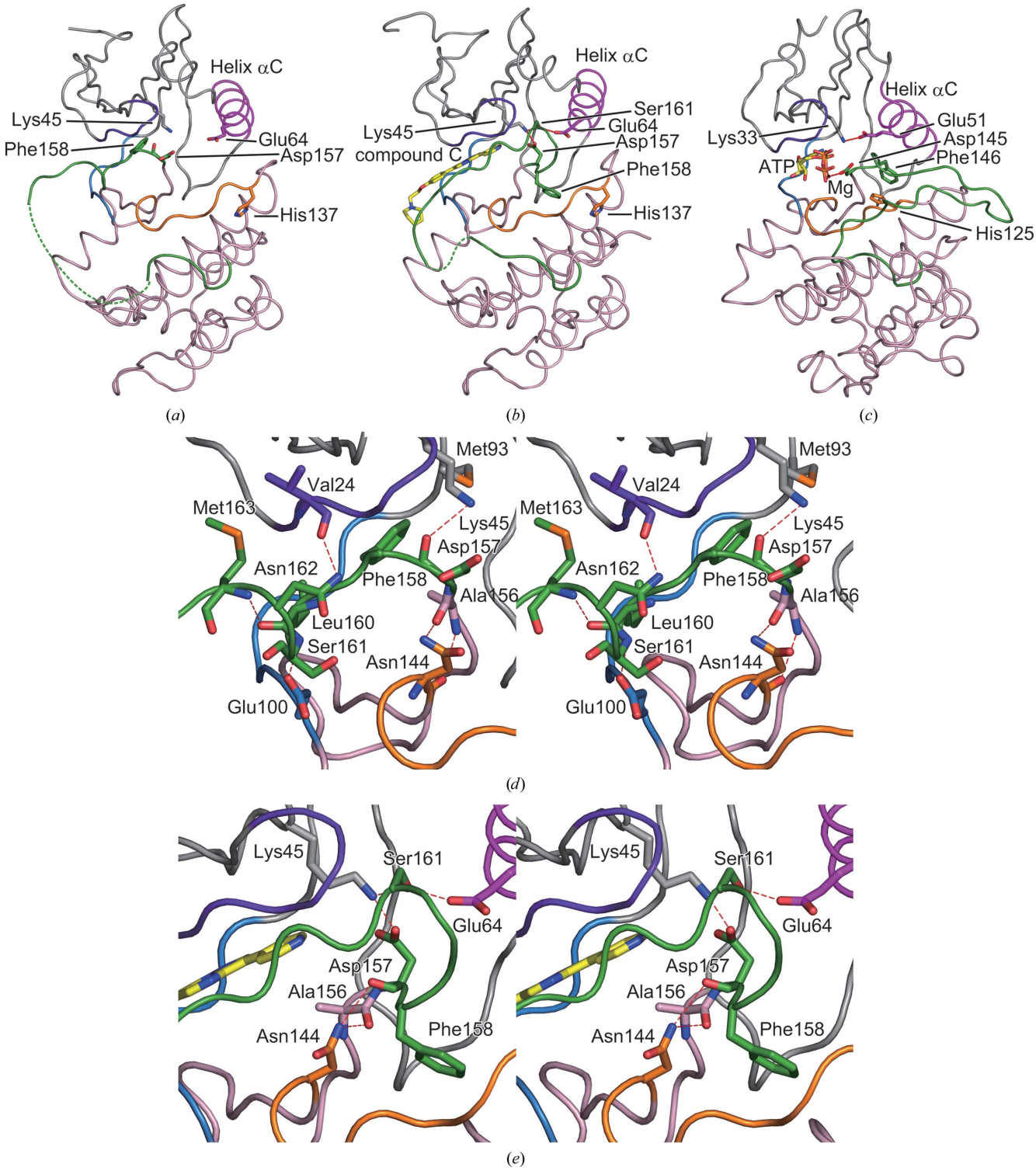

Figure 3
Activation-loop conformation. (*a*) Autoinhibited DFG-out conformation of the apo AMPK α2 T172D mutant. The glycine-rich loop, helix αC, the hinge, the catalytic loop and the activation loop are coloured purple, magenta, blue, orange and green, respectively. Other N-lobe and C-lobe regions are shown in white and pink, respectively. The disordered regions are represented by dotted lines. Lys45 in the glycine-rich loop, Glu64 in helix αC, His137 in the catalytic loop and Asp157 and Phe158 of the DFG motif in the activation loop are highlighted as stick models, with C, O and N atoms shown in yellow, red and blue, respectively. (*b*) Intermediate conformation between DFG-out and DFG-in of the compound-C-complexed AMPK α2 T172D mutant. The orientation and the colouring of the cartoon diagram are the same as in (*a*). The bound compound C molecule is represented by a yellow stick model. Hydrogen bonds are indicated by dashed red lines. (*c*) Activated and DFG-in conformation of CDK2 (PDB entry 1qmz; Brown *et al.*, 1999). The orientation and the colouring of the cartoon diagram are the same as in (*a*) and (*b*). The bound cAMP molecule is represented by a yellow stick model, with O, N and P atoms shown in red, blue and orange, respectively. The bound Mg is represented by a black sphere. (*d*) Close-up view of the DFG region of apo AMPK α2 (stereoview). The orientation and the colouring of the cartoon diagram are the same as in (*a*). (*e*) Close-up view of the DFG region of compound-C-complexed AMPK α2 (stereoview). The orientation and the colouring of the cartoon diagram are the same as in (*b*).

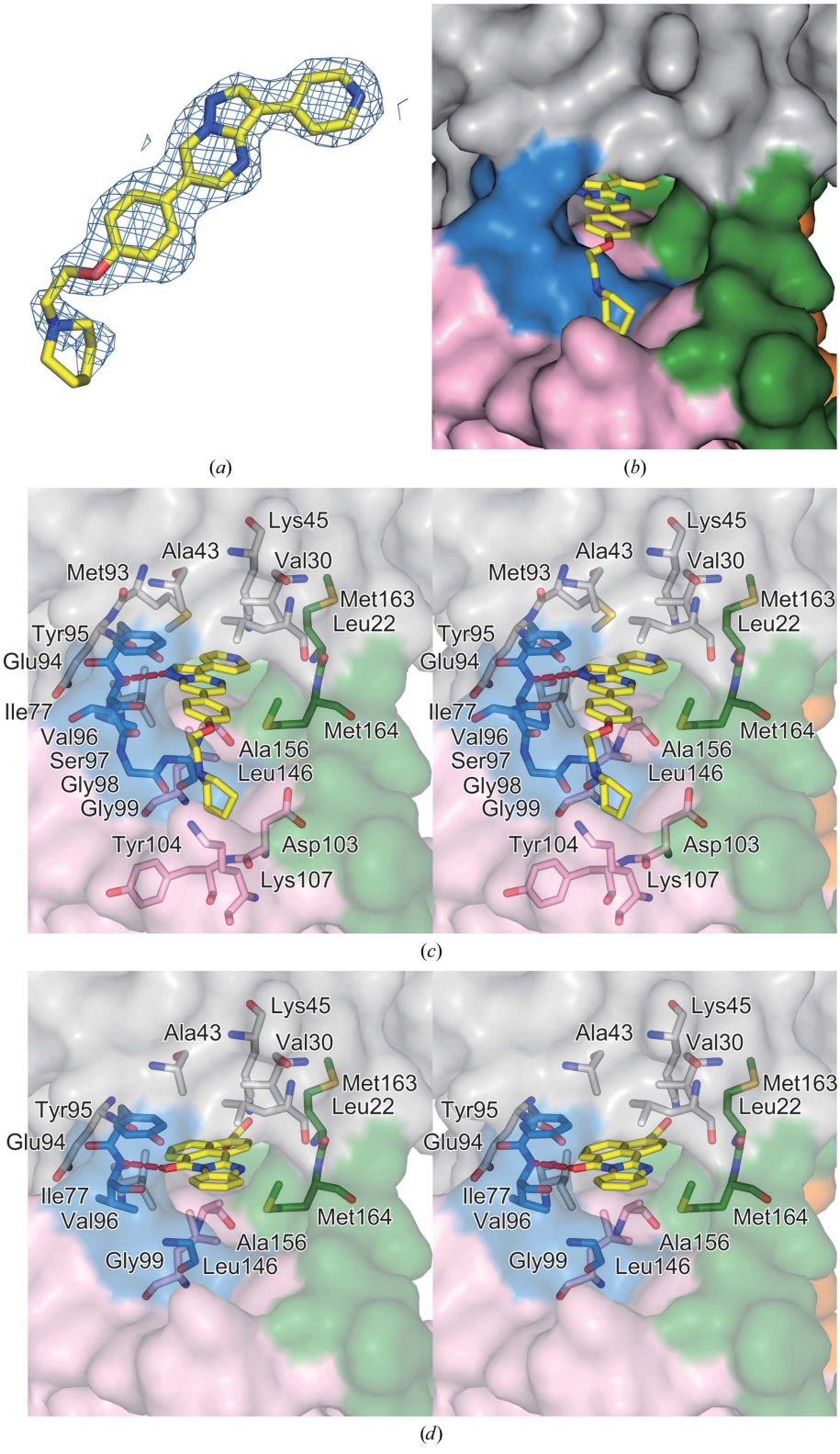

Figure 4
Compound C binding of AMPK α2. (*a*) A simulated-annealing OMIT $\alpha_{calc}(|F_o| - |F_c|)$ map was calculated without the compound C molecule atoms to 2.08 Å resolution and was contoured at 2.5σ. (*b*) A surface representation viewed from the opening of the compound-C binding pocket. The bound compound C is represented as a stick model. The colouring of the cartoon diagram is the same as in Fig. 3. (*c*) Stereo diagram showing the compound C recognition. The bound compound C and the interacting residues are shown as stick models. The colouring is the same as in (*b*). (*d*) Model of the compound-C binding pocket docked with STO 609 (stereoview). The bound STO 609 and the interacting residues are shown as stick models. The colouring is the same as in (*b*).

active kinases and forms a hydrogen bond to the main chain of Val96 (Figs. 3*b*, 3*c* and 4*c*).

The apo and compound-C-complexed structures superimpose well, but the structure of the activation loop, defined as the region between the conserved sequence motifs Asp-Phe-Gly (DFG) and Ala-Pro-Glu (APE), is significantly different (Figs. 1 and 2). The activation-loop conformation of the compound C complex is unique (Figs. 1*b* and 3*b*). Compared with the apo form, the N-terminal part of the activation loop moves toward the αC helix (Figs. 1, 3*a* and 3*b*). Asp157 of the DFG motif adopts an intermediate conformation between the DFG-out and DFG-in conformations ($\varphi_{\text{Asp157, AMPK }\alpha\text{2–compound C complex}} = -49^\circ$). The aromatic ring of Phe158 contacts the main chain of Arg-Asp-Leu (residues 138–140) in the catalytic loop (Fig. 3*b*). There are no contacts between Phe158 and His137. In the active state of the kinases, the DFG phenylalanine contacts the αC helix and the histidine side chain of the HRD motif in the catalytic loop, as also seen in the CDK2 structure (Fig. 3*c*).

The direct hydrogen bond between Lys and Glu seen in the active form is not formed in the compound C complex. However, the side chain of Ser161 is located between the side chains of Lys45 and Glu64 (Figs. 3*b* and 3*e*). Hydrogen bonds are formed between Ser161 and Lys45, Ser161 and Glu64, and Lys45 and Asp157 (Figs. 3*b* and 3*e*). These hydrogen bonds pull helix αC slightly inwards compared with the apo structure (Figs. 3*a* and 3*b*). In addition, the main-chain carbonyl O atoms of Ala156 and Asp157 form hydrogen bonds to the side chain of Asn144 (Fig. 3*e*). These interactions are completely different from those seen in the apo-form structure (Fig. 3*d*).

4. Discussion

In the absence of inhibitors such as compound C, the AMPK α2 kinase domain adopts the autoinhibited structure with the DFG-out conformation in both the wild-type (Littler *et al.*, 2010) and phosphorylated state-mimic T172D mutant (Fig. 3*a*) structures. The binding

of compound C alters the conformation of the activation loop and compound C is anchored within an elongated pocket that overlaps partially with the putative ATP-binding pocket.

The apo human AMPK α2 kinase domains of both the wild type and the phosphorylated-state mimic T172D mutant are monomers in the crystals. This is in contrast to the yeast homologue, Snf1, in which the unphosphorylated kinase domain forms a homodimer in the crystals and in solution and the phosphorylated kinase domain forms a monomer in solution (Nayak *et al.*, 2006; Rudolph *et al.*, 2005; Chen *et al.*, 2009). The homodimerization of Snf1 buries the activation loop and the substrate-binding site and thus represents an inactive conformation of the kinase (Nayak *et al.*, 2006). According to the crystal structures, the human AMPK α2 kinase domain does not seem to use regulatory mechanisms similar to those seen in the yeast Snf1 homodimer structure. Instead, the human AMPK α2 kinase autoinhibits by adopting the DFG-out conformation. The autoinhibitory domain, residues 289–336, following the kinase domain may contribute to the stabilization of this DFG-out autoinhibitory structure (Pang *et al.*, 2007; Chen *et al.*, 2009). The conformation of the activation loop in the *S. pombe* AMPK α KD-AID crystal structure may be a consequence of crystal packing, as several residues in the activation loop form intramolecular and intermolecular contacts at the artificial homodimer interface (Chen *et al.*, 2009). The recently solved crystal structure of the yeast Snf1 KD-AID revealed a DFG-out conformation, which would allow the glycine-rich loop to interfere with ATP binding (Rudolph *et al.*, 2010). Therefore, the autoinhibitory mechanism of AMPK and Snf1 by adoption of the DFG-out conformation may be conserved across eukaryotic species.

AMPK α2 activation is mediated by the phosphorylation of Thr172 located in the activation loop (Hardie *et al.*, 2006). Since the phosphothreonine-mimic Asp172 and its neighbouring amino acids were not visible in the electron-density map, they are probably flexible and unstructured. AMPK is a heterotrimer consisting of a catalytic α subunit and regulatory β and γ subunits. The phosphorylated and/or unphosphorylated Thr172 may interact with residues in the regulatory subunits which stabilize the kinase-domain conformation in either the active or inactive mode. Although the α, β and γ subunit complex structures of mammalian AMPK and the yeast homologues have been published (Amodeo *et al.*, 2007; Townley & Shapiro, 2007; Xiao *et al.*, 2007; Jin *et al.*, 2007), none of them contain the kinase domain. Further studies are needed to elucidate the molecular mechanisms of the regulation by phosphorylation of the activation loop.

Compound C is bound tightly in a unique elongated binding pocket and it stabilizes the kinase-domain structure in the crystal. NMR and thermal stability studies revealed that the free AMPK α2 kinase domain is easily unfolded and that the addition of compound C to the protein solution stabilizes the protein folding (data not shown). In the crystal, the activation loop is more stable in the compound-C-complexed form. However, the major regulatory phosphorylation site Thr172 located in the activation loop is flexible and extended in solution, even though Thr172 is mutated to Asp. Recent reports revealed that compound C affects AMPK phosphorylation (McCullough *et al.*, 2005; Fediuc *et al.*, 2006). The unique conformation of the activation loop induced and stabilized by compound C could reduce the phosphorylation of Thr172 by AMPK kinases and/or promote the dephosphorylation of Thr172 by protein phosphatases.

AMPK is also inhibited, with similar potency, by the selective CaMKK2 inhibitor STO 609 (Bain *et al.*, 2007). As no three-dimensional structure of AMPK in complex with STO 609 was available, we used a molecular-docking algorithm to predict the binding mode (Fig. 4*d*). STO 609 fits well in the compound-C binding pocket and binds in a similar orientation to CaMKK2 (PDB entry 2zv2; our unpublished results). STO 609 forms similar hydrophobic contacts as the pyridinyl-pyrazolopyrimidine ring of compound C (Figs. 4*c* and 4*d*).

Compound C also inhibits bone morphogenetic protein (BMP) signals by blocking the kinase functions of the BMP type I receptors ALK2, ALK3 and ALM6 (Yu *et al.*, 2008). The crystal structure of the kinase domain of ALK2 in complex with FKBP12 and compound C has recently become available in the Protein Data Bank (PDB entry 3h9r; Structural Genomics Consortium, unpublished work). Compound C binds to ALK2 in a similar region to that bound by compound C in AMPKα2 formed by the N-lobe, the C-lobe and the hinge of the kinase domain.

Our structures presented here provide the structural basis for understanding the mechanism of AMPK inhibition by compound C and will facilitate the design of specific modulators of AMPK activity. We employed a structure-based *in silico* screening approach in combination with cell-based and biochemical assays. Our preliminary data suggest that several compounds thus identified possess more specific AMPK inhibition activity than compound C.

Note added in proof. Recently, the crystal structure of the mammalian AMPK heterotrimer, which consists of the full-length α subunit, residues 187–272 of the β subunit, and the full-length γ subunit, was published (Xiao *et al.*, 2011).

We thank Yukiko Kinoshita, Seiko Yoshikawa, Tomomi Uchikubo-Kamo and Ryogo Akasaka for technical assistance and Mitsuo Kuratani for comments on the manuscript. This work was supported by the RIKEN Structural Genomics/Proteomics Initiative (RSGI), the National Project on Protein Structural and Functional Analyses and the Targeted Proteins Research Program (TPRP) of the Ministry of Education, Culture, Sports, Science and Technology of Japan.

References

Alessi, D. R., Sakamoto, K. & Bayascas, J. R. (2006). *Annu. Rev. Biochem.* **75**, 137–163.

Amodeo, G. A., Rudolph, M. J. & Tong, L. (2007). *Nature (London)*, **449**, 492–495.

Bain, J., Plater, L., Elliott, M., Shpiro, N., Hastie, C. J., McLauchlan, H., Klevernic, I., Arthur, J. S., Alessi, D. R. & Cohen, P. (2007). *Biochem. J.* **408**, 297–315.

Brown, N. R., Noble, M. E., Endicott, J. A. & Johnson, L. N. (1999). *Nature Cell Biol.* **1**, 438–443.

Brünger, A. T., Adams, P. D., Clore, G. M., DeLano, W. L., Gros, P., Grosse-Kunstleve, R. W., Jiang, J.-S., Kuszewski, J., Nilges, M., Pannu, N. S., Read, R. J., Rice, L. M., Simonson, T. & Warren, G. L. (1998). *Acta Cryst.* D**54**, 905–921.
Chen, L., Jiao, Z.-H., Zheng, L.-S., Zhang, Y.-Y., Xie, S.-T., Wang, Z.-X. & Wu, J.-W. (2009). *Nature (London)*, **459**, 1146–1149.
Cheung, P. C., Salt, I. P., Davies, S. P., Hardie, D. G. & Carling, D. (2000). *Biochem. J.* **346**, 659–669.
Fediuc, S., Gaidhu, M. P. & Ceddia, R. B. (2006). *J. Lipid Res.* **47**, 412–420.
Fogarty, S. & Hardie, D. G. (2010). *Biochem. Biophys. Acta*, **1804**, 581–591.
Friesner, R. A., Banks, J. L., Murphy, R. B., Halgren, T. A., Klicic, J. J., Mainz, D. T., Repasky, M. P., Knoll, E. H., Shelley, M., Perry, J. K., Shaw, D. E., Francis, P. & Shenkin, P. S. (2004). *J. Med. Chem.* **47**, 1739–1749.
Gouet, P., Courcelle, E., Stuart, D. I. & Métoz, F. (1999). *Bioinformatics*, **15**, 305–308.
Hardie, D. G. (2007). *Nature Rev. Mol. Cell Biol.* **8**, 774–785.
Hardie, D. G., Hawley, S. A. & Scott, J. W. (2006). *J. Physiol.* **574**, 7–15.
Hawley, S. A., Pan, D. A., Mustard, K. J., Ross, L., Bain, J., Edelman, A. M., Frenguelli, B. G. & Hardie, D. G. (2005). *Cell Metab.* **2**, 9–19.
Hurley, R. L., Anderson, K. A., Franzone, J. M., Kemp, B. E., Means, A. R. & Witters, L. A. (2005). *J. Biol. Chem.* **280**, 29060–29066.
Jin, X., Townley, R. & Shapiro, L. (2007). *Structure*, **15**, 1285–1295.
Kannan, N. & Neuwald, A. F. (2005). *J. Mol. Biol.* **351**, 956–972.
Kigawa, T., Yabuki, T., Matsuda, N., Matsuda, T., Nakajima, R., Tanaka, A. & Yokoyama, S. (2004). *J. Struct. Funct. Genomics*, **5**, 63–68.
Kigawa, T., Yabuki, T. & Yokoyama, S. (1999). *Tanpakushitsu Kakusan Koso*, **44**, 598–605.
Kigawa, T., Yabuki, T., Yoshida, Y., Tsutsui, M., Ito, Y., Shibata, T. & Yokoyama, S. (1999). *FEBS Lett.* **442**, 15–19.
Kim, E.-K., Miller, I., Aja, S., Landree, L. E., Pinn, M., McFadden, J., Kuhajda, F. P., Moran, T. H. & Ronnett, G. V. (2004). *J. Biol. Chem.* **279**, 19970–19976.
Li, J., Zeng, Z., Viollet, B., Ronnett, G. V. & McCullough, L. D. (2007). *Stroke*, **38**, 2992–2999.
Littler, D. R., Walker, J. R., Davis, T., Wybenga-Groot, L. E., Finerty, P. J., Newman, E., Mackenzie, F. & Dhe-Paganon, S. (2010). *Acta Cryst.* F**66**, 143–151.
McCullough, L. D., Zeng, Z., Li, H., Landree, L. E., McFadden, J. & Ronnett, G. V. (2005). *J. Biol. Chem.* **280**, 20493–20502.
Minokoshi, Y., Alquier, T., Furukawa, N., Kim, Y.-B., Lee, A., Xue, B., Mu, J., Foufelle, F., Ferré, P., Birnbaum, M. J., Stuck, B. J. & Kahn, B. B. (2004). *Nature (London)*, **428**, 569–574.
Minokoshi, Y., Kim, Y.-B., Peroni, O. D., Fryer, L. G., Müller, C., Carling, D. & Kahn, B. B. (2002). *Nature (London)*, **415**, 339–343.
Momcilovic, M., Hong, S.-P. & Carlson, M. (2006). *J. Biol. Chem.* **281**, 25336–25343.
Nayak, V., Zhao, K., Wyce, A., Schwartz, M. F., Lo, W.-S., Berger, S. L. & Marmorstein, R. (2006). *Structure*, **14**, 477–485.
Otwinowski, Z. & Minor, W. (1997). *Methods Enzymol.* **276**, 307–326.
Pang, T., Xiong, B., Li, J.-Y., Qiu, B.-Y., Jin, G.-Z., Shen, J.-K. & Li, J. (2007). *J. Biol. Chem.* **282**, 495–506.
Pargellis, C., Tong, L., Churchill, L., Cirillo, P. F., Gilmore, T., Graham, A. G., Grob, P. M., Hickey, E. R., Moss, N., Pav, S. & Regan, J. (2002). *Nature Struct. Biol.* **9**, 268–272.
Rudolph, M. J., Amodeo, G. A., Bai, Y. & Tong, L. (2005). *Biochem. Biophys. Res. Commun.* **337**, 1224–1228.
Rudolph, M. J., Amodeo, G. A. & Tong, L. (2010). *Acta Cryst.* F**66**, 999–1002.
Scott, J. W., Norman, D. G., Hawley, S. A., Kontogiannis, L. & Hardie, D. G. (2002). *J. Mol. Biol.* **317**, 309–323.
Stapleton, D., Mitchelhill, K. I., Gao, G., Widmer, J., Michell, B. J., Teh, T., House, C. M., Fernandez, C. S., Cox, T., Witters, L. A. & Kemp, B. E. (1996). *J. Biol. Chem.* **271**, 611–614.
Suzuki, A., Kusakai, G., Kishimoto, A., Shimojo, Y., Ogura, T., Lavin, M. F. & Esumi, H. (2004). *Biochem. Biophys. Res. Commun.* **324**, 986–992.
Suzuki, A., Kusakai, G., Shimojo, Y., Chen, J., Ogura, T., Kobayashi, M. & Esumi, H. (2005). *J. Biol. Chem.* **280**, 31557–31563.
Suzuki, A., Okamoto, S., Lee, S., Saito, K., Shiuchi, T. & Minokoshi, Y. (2007). *Mol. Cell. Biol.* **27**, 4317–4327.
Ten Eyck, L. F., Taylor, S. S. & Kornev, A. P. (2008). *Biochim. Biophys. Acta*, **1784**, 238–243.
Townley, R. & Shapiro, L. (2007). *Science*, **315**, 1726–1729.
Vagin, A. & Teplyakov, A. (2010). *Acta Cryst.* D**66**, 22–25.
Wada, T., Shirouzu, M., Terada, T., Ishizuka, Y., Matsuda, T., Kigawa, T., Kuramitsu, S., Park, S.-Y., Tame, J. R. H. & Yokoyama, S. (2003). *Acta Cryst.* D**59**, 1213–1218.
Winn, M. D., Isupov, M. N. & Murshudov, G. N. (2001). *Acta Cryst.* D**57**, 122–133.
Woods, A., Dickerson, K., Heath, R., Hong, S.-P., Momcilovic, M., Johnstone, S. R., Carlson, M. & Carling, D. (2005). *Cell Metab.* **2**, 21–33.
Xiao, B., Heath, R., Saiu, P., Leiper, F. C., Leone, P., Jing, C., Walker, P. A., Haire, L., Eccleston, J. F., Davis, C. T., Martin, S. R., Carling, D. & Gamblin, S. J. (2007). *Nature (London)*, **449**, 496–500.
Xiao, B. *et al.* (2011). *Nature (London)*. doi:10.1038/nature09932.
Yamauchi, T. *et al.* (2002). *Nature Med.* **8**, 1288–1295.
Yu, P. B., Hong, C. C., Sachidanandan, C., Babitt, J. L., Deng, D. Y., Hoyng, S. A., Lin, H. Y., Bloch, K. D. & Peterson, R. T. (2008). *Nature Chem. Biol.* **4**, 33–41.
Zhou, G., Myers, R., Li, Y., Chen, Y., Shen, X., Fenyk-Melody, J., Wu, M., Ventre, J., Doebber, T., Fujii, N., Musi, N., Hirshman, M. F., Goodyear, L. J. & Moller, D. E. (2001). *J. Clin. Invest.* **108**, 1167–1174.